

Adsorption of phosphate from solution by iron modified macroporous chelating resin

Xiaoting Zhang, Ruize Zhang, Shanshan Chen, Kang Wen, Runping Han*

College of Chemistry and Molecular Engineering, Zhengzhou University, No 100 of Kexue Road, Zhengzhou, 450001 China, Tel. +86 371 67781757; Fax: +86 371 67781556; emails: rphan67@zzu.edu.cn (R.P. Han), 1619888517@qq.com (X.T. Zhang), 690724768@qq.com (R. Zhang), 2503579590@qq.com (S.S. Chen), 1039171416@qq.com (K. Wen)

Received 2 April 2019; Accepted 8 July 2019

ABSTRACT

In this study, D751 resin (macroporous styrene chelated ion exchange resin, sodium form) was modified by FeCl_3 to enhance the adsorption performance of phosphate from solution. The modified resin (D751-Fe) was characterized by FTIR and XPS, and its adsorption property toward phosphate was presented. The results showed that it was favorable of phosphate adsorption with the increase in the temperature and acidity. The effect of coexisting ions (chloride and sulfate) was insignificant. When the solid–liquid ratio was 1.5 g L^{-1} , the unit adsorption amount of D751-Fe toward phosphate was to 14.1 mg g^{-1} (according to P element) with solution pH 3. The adsorption isotherms were well fitted by Langmuir model, Freundlich model, and Koble–Corrigan model while the kinetic curves were well described by pseudo-first-order kinetic model, double constant model, and intraparticle model. There were both physical adsorption and chemical adsorption between D751-Fe and phosphate. It was effective for 0.1 mol-L^{-1} sodium hydroxide solution as desorbent to regenerate phosphate-loaded adsorbent. It is concluded that that D751-Fe can be used well for the removal of phosphate from solution.

Keywords: Phosphate; Iron-modified D751 resin; Adsorption; Regeneration

1. Introduction

Phosphorus is an essential nutrient for the growth of animals and plants, and is expressed in all aspects of our lives [1,2]. However, it has become one of the main causes of eutrophication of water bodies as the large amount of phosphorus-containing wastewater produced by food processing, the production and use of detergents, and the use of phosphorus fertilizers and organophosphorus pesticides [3–6]. Excessive phosphorus content not only harms water bodies, soils, and plants but also affects human health and even life safety.

At present, the methods for removal of phosphorus mainly include chemical methods [7], biological methods [8,9], and adsorption methods [10–13]. Among them,

chemical method is not only costly but also the metal salt used in the removal process will cause secondary pollution to the environment, for example, using barium hydroxide to adsorb phosphate with higher reagent cost [14]. Biological treatment of phosphorus-containing wastewater has strict requirements on biological living conditions and wastewater quality. However, adsorption method has the advantages of simple operation, low processing cost, high phosphorus removal efficiency and is widely used in remediation field. So finding low-cost, high-efficiency adsorbents is a hot topic in recent years. In addition to the above advantages, the resin has a high degree of functionalization and good selectivity, and can be applied in the water treatment. At present, it has been widely used in the preparation process of Chinese herbal medicine to remove excess heavy metals (such as copper, tungsten, arsenic), or to be used for the adsorption of anions (such as ammonia nitrogen and fluorine in

* Corresponding author.

wastewater) in water bodies by transition metal modification and so on [15–21]. However, there are not many reports on phosphorus removal by resins. Xie et al. [22] used cation exchange resin loaded nano-scale zero-valent iron to remove phosphorus in rainwater runoff; the study pointed out that 0.72 mg L⁻¹ of phosphorus could be reduced to 0.42 mg L⁻¹. Ye et al. [23] used DS ion exchange resin to remove and recover phosphorus from eutrophic river water, the saturated adsorption capacity of DS in the soluble orthophosphate reached 1.3 mg g⁻¹ and the saturated adsorption capacity of total phosphorus reached 1.8 mg g⁻¹. The unit adsorption capacity still needs to be improved. So, there is still a gap between these and our expectations. There are possible prospects for exploring new ways for advanced treatment and recycling of phosphate from phosphate-containing wastewater, further packed and used for commercial water purification for the benefit of mankind. The problem of the utilization ratio of the resin, the saturated adsorption amount of phosphorus, and the removal efficiency of phosphorus are comprehensively considered. Anionic exchangeable resin can be directly used to exchange phosphate from solution, but the efficiency is significantly decreased if there are more coexisted common ions in solution. As common knowledge, if interaction between adsorbent and phosphate is main complex or coordination, there will be little effect with the common salts in solution. D751 resin as a macroporous styrene-based chelating resin (functional base: sodium N, N-iminodiacetic acid) was used in the research of this subject. D751 resin has the characteristics of high degree of functionalization, large degree of crosslinking and stable load. At present, it is widely used to adsorb cations, such as adsorption of lithium ions [24]. However, there are fewer reports on phosphate removal by modified D751 resin. In this study, the iron-modified D751 resin significantly improved adsorption quantity toward some pollutants from solution.

FeCl₃ is inexpensive and easily obtained and it is also environmental friendly [25]. It is considered to be an electron pair acceptor as its strong Lewis acid properties, and has a strong affinity toward phosphate. In the investigation of this experiment, D751 resin was modified by iron, and the modified resin (D751-Fe) was characterized and the adsorption property toward phosphate was investigated. Several adsorption models were applied and the regeneration of spent D751-Fe was performed.

2. Materials and methods

2.1. Materials

Ferric chloride (FeCl₃·6H₂O) was purchased from Tianjin Damao Chemical Reagent Factory (China); anhydrous ethanol (C₂H₅OH) was derived from Fuchen (Tianjin) Chemical Reagent Co., Ltd.; hydrochloric acid (HCl) was exported to Yantai Shuangshuang Chemical Co. Ltd. Company (China); sodium hydroxide (NaOH) was purchased from Yantai Shuangshuang Chemical Co., Ltd.; sodium chloride (NaCl) was obtained from Anhui Suzhou Chemical Reagent Factory (China); potassium dihydrogen phosphate (KH₂PO₄) was acquired from Beijing Chemical Plant (China); D751 resin (macroporous chelating ion exchange resin, sodium form; the granularity: 0.3–1.2 mm ≥95%; the moisture content

(Na⁺ type): 57.000000%) was derived from Aladdin (Shanghai, China); the above reagents were of analytical grade; the experimental water was deionized water.

2.2. Instrument

The main instruments used in this study are following: the concentration of phosphate was measured using a UV-visible spectrophotometer (752 Shanghai Hanyu Hengping Instrument Co. Ltd., China) with a 1 cm path length according to the Beer–Lambert law at a wavelength corresponding to the maximum absorbance at 700 nm (the molybdenum blue method); the pH of solutions was measured with a precision acidity meter (PHS-3C Shanghai Scientific Instrument, China) at room temperature; all reactions were carried out in a constant temperature oscillator (SHZ-82 Changzhou Guohua Electric Co. Ltd., China) at constant speed (120 rpm); drying of the material in a constant temperature drying oven (202-V1 Shanghai Experimental Instrument Factory, China).

2.3. Preparation of iron-loaded modified D751 resin

2.3.1. D751 resin pretreatment

The D751 resin was pretreated according to the existing literature and combined with individual experimental conditions [26]. A certain amount of resin was immersed in four times resin volume of absolute ethanol for 24 h (for completely dissolving the organic matter on the surface of the resin), then washed with deionized water to tasteless to remove organic impurities on the surface; then four times resin volume of 1 mol L⁻¹ HCl and NaOH by the order of HCl–NaOH–HCl were alternately soaked for 24 h to wash dirty materials (making it fully activated, the pH is measured by an acidity meter during the acid–base treatment. the ion exchange was considered complete until the pH was not changing. This amount was sufficient to make the exchange completely). Finally, the resin was washed with deionized water to neutrality, then H-type resin was obtained after dried at 60°C under vacuum for 12 h, which was denoted as D751-H.

2.3.2. D751 resin-loaded iron

A certain mass of D751-H was put into a 4-fold resin volume of 0.2 mol L⁻¹ FeCl₃ solution, and shaken in a constant temperature water bath at 40°C, 120 rpm for 12 h. During the process of oscillating, the solution was slowly adjusted with a 1.0 mol L⁻¹ NaOH solution to adjust the pH to 2.0 (reducing the acidity was beneficial to the load, while avoiding the precipitation of Fe³⁺, so the pH was adjusted to 2.0) and the FeCl₃ solution was replaced four times (making it fully loaded). Finally, the resin was washed with distilled water to neutrality and dried in a vacuum oven at 60°C for 12 h, which was designated as D751-Fe.

2.4. Characterization of the adsorbent

In order to understand the performance of the adsorbent, a series of characterizations were carried out: FTIR analysis (PE-1710FTIR American PE Company, (Chinese Company) (Guangzhou, China)) was used to determine the loading

form of Fe on the adsorbent with KBr as the salt window and the air as blank. Photoelectric energy spectrum (Escalab 250Xi, Thermo Fisher, UK) was adopted to judge the change in the surface elements of the adsorbent before and after adsorption.

The isoelectric point of the adsorbent was determined by using 0.01 mol L⁻¹ NaCl. 0.03 g of D751-Fe was placed in a series of 50 mL conical flasks containing 20 mL of 0.01 mol L⁻¹ NaCl (pH₀ = 2–12), and shaken in a constant temperature water bath at 30°C, 120 rpm for 15 h. The pH difference before and after the solution is the ΔpH, which is plotted with pH₀ as the abscissa and ΔpH as the ordinate, then the intersection with the abscissa is the isoelectric point of the adsorbent.

2.5. Adsorption experiment

In this experiment, the adsorption performance of D751-Fe toward phosphate was investigated by a series of experiments. By taking a certain amount of adsorbent in a series of 50 mL conical flasks, 20 mL phosphate solution with a certain concentration of (concentration as P) was added. Then the mixture was shaken in a constant temperature water bath at a certain temperature, 120 rpm for a certain time, respectively. The effects of solution pH (2–11), adsorbent dosage (0.01–0.10 g), salinity (0–0.20 mol L⁻¹ NaCl and Na₂SO₄), initial solution concentration (10, 20, 30 mg L⁻¹), contact time (0–12 h) and adsorption temperature (20°C, 30°C, 40°C) on the adsorption of phosphate onto D751-Fe were researched. Among them, the pH of the solution was adjusted with a certain concentration of NaOH and HCl, and was measured with a pH meter. The concentration of the solution after adsorption was calculated by measuring the absorbance at 700 nm by molybdenum rhenium anti-spectrophotometry.

The unit adsorption amount and removal rate were calculated by Eqs. (1) and (2), respectively.

$$q_e = \frac{V(C_0 - C_e)}{m} \quad (1)$$

$$p = \frac{(C_0 - C_e)}{C_0} \times 100\% \quad (2)$$

where q_e (mg g⁻¹) denotes the unit adsorption amount (according to P element), m (g) means the weight of the adsorbent, V (L) shows the volume of the adsorbate solution, p (%) represents the removal efficiency and C_0 (mg L⁻¹) indicates the adsorbate concentration before adsorption, C_e (mg L⁻¹) signifies the adsorbate concentration after adsorption.

Adsorption experiments were repeated at three times and averages were recorded. The error is less than 5%.

2.6. Adsorption kinetics

Accurately pipetted 20 mL of a 10, 20, 30 mg L⁻¹ phosphate solution (pH = 3.0) into a series of 50 mL conical flasks. Then, 0.03 g of D751-Fe was added, respectively, and shaken in a constant temperature water bath at 20°C, 30°C, 40°C, 120 rpm for a certain time. The unit adsorption amount was taken out at different times.

2.7. Isothermal adsorption study

20 mL of different concentrations of phosphate solution (pH = 3.0) was accurately transferred into a series of 50 mL conical flask. Then, 0.03 g of D751-Fe was added, respectively, and shaken in a constant temperature water bath at 20°C, 30°C, 40°C, 120 rpm for 18 h. Then phosphate concentration of solution was measured.

2.8. Desorption and regeneration experiments

In order to better explain the adsorption mechanism and judge the economic benefit of the adsorbent, the static desorption regeneration experiment of the adsorbent after adsorption was carried out by different desorption methods. First, 0.03 g of D751-Fe was accurately weighed into a series of 50 mL conical flasks containing 20 mL phosphate solution (30 mg L⁻¹, pH = 3.0), and shaken in a constant temperature water bath at 30°C, 120 rpm for 12 h. Then adsorbent was washed with deionized water for several times and drying in a vacuum drying oven for 12 h, then P-loaded or spent D751-Fe was obtained; and the unit adsorption amount q_e was calculated. Then, 20 mL of 0.1 mol L⁻¹ NaOH was added to the conical flask containing 0.03 g of spent adsorbent, and shaken in a constant temperature water bath at 30°C for 12 h; the desorption efficiency d was calculated. Finally, the desorbed adsorbent was washed with deionized water and then regenerated. The method was the same as above, and the regeneration efficiency r was calculated. The desorption efficiency and the regeneration efficiency were determined as Eqs. (3) and (4), respectively.

$$d = \frac{m_d}{m_0} \times 100\% \quad (3)$$

$$r = \frac{q_n}{q_0} \times 100\% \quad (4)$$

where d (%) is the desorption efficiency, r (%) represents the regeneration efficiency, m_d (g) means the mass of the adsorbed material desorbed, m_0 (g) is the mass of the adsorbate on the adsorbent after adsorption, q_n (mg g⁻¹) indicates the unit adsorption amount when adsorbed again (n is the number of regeneration times), and q_0 (mg g⁻¹) denotes the unit adsorption amount before desorption.

In order to explore the reaction mechanism of the desorption process, analytical kinetic experiments were carried out. 0.03 g of the adsorbed adsorbent was placed in a series of 50 mL conical flasks containing 20 mL of 0.1 mol L⁻¹ NaOH desorption solution, and shaken in a constant temperature water bath at 30°C, 120 rpm for different time. The desorption efficiency was calculated by taking out the desorbed solution at different time.

3. Results and discussion

3.1. Characterization of materials

3.1.1. FTIR analysis

In order to compare the changes of surface functional groups before and after resin modification, the FTIR spectra

of the resin before and after modification are analyzed. Fig. 1 shows the FTIR spectrum of D751-H and D751-Fe. Comparing the FTIR spectra of the resin before and after modification, it was seen that there was an absorption peak at 709 cm^{-1} for modified resin, which was a characteristic absorption peak of Fe-O bond [27], and this indicated that the iron had been successfully loaded onto D751. The stretching vibration peak of the carbonyl group at $1,729\text{ cm}^{-1}$ was

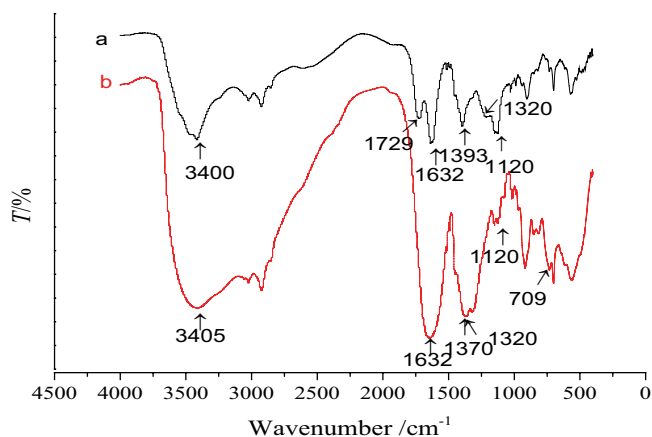


Fig. 1. FTIR spectra of D751-H (a) and D751-Fe (b).

weakened or covered after modification, which might also be due to the binding of oxygen (adjacent the carboxyl group) to form a coordination bond with iron; $3,400$ and $1,632\text{ cm}^{-1}$ were characteristic absorption peaks of $-\text{OH}$ [28], and the peak shape here was broadened after modification, which might be due to the presence of an associated hydroxyl group on the iron. After modification, there was an absorption peak at $1,370\text{ cm}^{-1}$, which was the deformation vibration of $\text{O}-\text{H}$ [29]. It might also be due to the presence of associative hydroxyl groups on the iron. The bands at $1,320\text{ cm}^{-1}$ represented the $\text{C}-\text{N}$ stretching vibration, and the peak shape was enhanced after modification, which might be due to the formation of a coordination bond between N and Fe . In summary, Fe was loaded in the form of complexation.

3.1.2. XPS analysis

In order to judge the change of surface elements before and after adsorption of adsorbent, and analyze it qualitatively, the adsorbents before and after adsorption are analyzed with XPS (charge correction was performed using standard C and Shirley background adjustment was used on the spectra), and the results are shown in Fig. 2. It is seen from Fig. 2 that XPS of D751-Fe before adsorption showed that the binding energies of $\text{C } 1s$, $\text{N } 1s$, $\text{O } 1s$ and $\text{Fe } 2p$ were 285.45 , 400.66 , 532.08 and 712.72 eV , respectively. The adsorbent after adsorption increased the photoelectron peak of 133.67 eV P

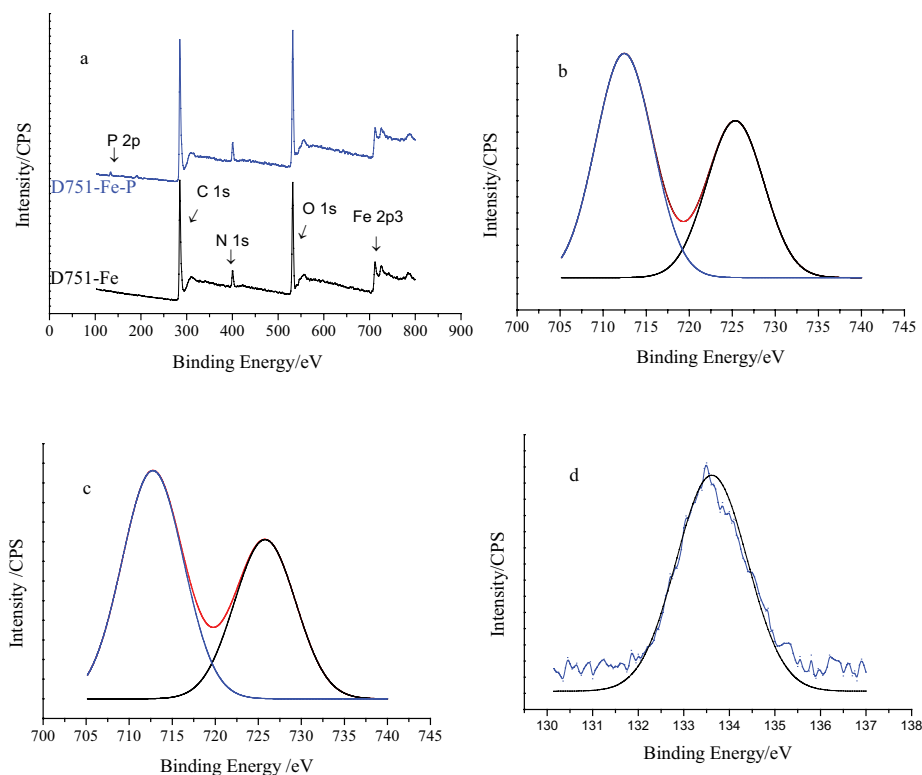


Fig. 2. (a) Full spectrum of XPS before and after adsorption of phosphate; (b) high-resolution XPS spectrum of $\text{Fe } 2p$ before adsorption of phosphate; (c) high-resolution XPS spectrum of $\text{Fe } 2p$ after adsorption of phosphate; (d) high-resolution XPS spectrum of $\text{P } 2p$ after adsorption of phosphate.

2p relative to that before adsorption. In addition, the photoelectron peak of O 1s was enhanced. It revealed that P was successfully adsorbed on the adsorbent.

In order to further explore the changes of the surface groups of the adsorbent before and after adsorption, the Fe 2p and P 2p characteristic peaks are partially scanned. The results are also shown in Fig. 2. It is observed from Fig. 2 that there were two absorption peaks at 712.45 and 725.36 eV before adsorption, which were Fe 2p_{3/2} and Fe 2p_{1/2}, respectively; the contents were 58.82% and 41.18%, respectively. After adsorption, the two absorption peaks were shifted to 712.74 and 725.79 eV, respectively, and the contents were 58.91% and 41.09%, respectively. The reason might be that the bond energy was slightly enhanced due to the formation of Fe-O-P bond through phosphate adsorption [30,31]. It can be found from Fig. 2 that a new peak appeared at 133.6 eV after the adsorption of phosphate, which corresponded to P2p, indicated phosphate in the PO₄ group structure [30,31]. This suggested that phosphate be adsorbed on the surface of the adsorbent by forming a complex with iron [31].

3.1.3. Determination of isoelectric point

In order to determine the electrical properties of the adsorbent surface, an isoelectric point test can be performed. The pH difference before and after the measurement is the ΔpH , which is plotted against pH_0 , and the intersection of the curves is the isoelectric point of the material. The results are shown in Fig. 3. It is observed from Fig. 3 that the isoelectric point of the D751-Fe was about 4.0 and this showed the surface with positive charge at $\text{pH} < 4.0$ or with negative charge at $\text{pH} > 4.0$. This was a good indication of why D751-Fe readily adsorbed phosphate under acidic conditions.

3.2. Adsorption study

3.2.1. Effect of pH

Solution pH often plays an important role in the adsorption process as it can affect the surface chemical and physical properties of adsorbent and the existing form of adsorbate in solution. Therefore, this experiment explores the effect of solution pH on the phosphate uptake by D751-H and D751-Fe and the results are presented in Fig. 4. It is clearly observed from the figure that there was nearly no adsorption capacity toward phosphate about D751-H and the adsorption capacity was obviously improved after

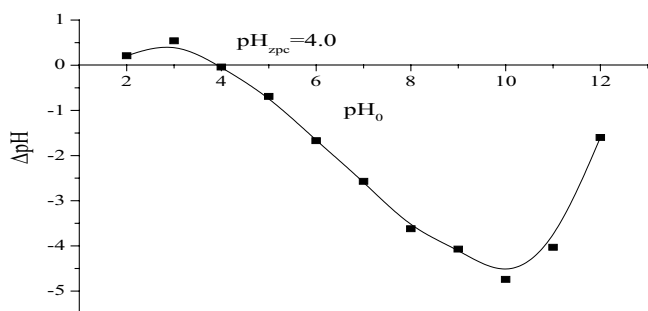


Fig. 3. Isoelectric point of D751-Fe.

Fe loading. The adsorption quantity of D751-Fe showed a downward trend with pH in the range of 2–11. When the pH value was between 2.0 and 3.0, the unit adsorption amount changed insignificantly, and the unit adsorption amount was largest. Then the adsorption amount decreased rapidly with the pH from 3.0 to 8.0. When the pH value was between 8.0 and 11.0, the unit adsorption amount tended to be stable. The possible reasons for this phenomenon were as follows: (1) phosphate was mainly present in the form of dihydrogen phosphate under acidic conditions, and the form was easily adsorbed by the adsorbent; (2) the adsorbent surface was positively charged under acidic conditions, and tended to act with negatively charged phosphate; (3) the OH⁻ content in the solution increased with the acidity decreased, and there was competitive adsorption with phosphate, while there was also electrostatic repulsion between adsorbent and phosphate [30]. Zhang et al. studied the removal of phosphorus onto hydrazine-containing carboxymethyl konjac glucomannan from slaughter wastewater and the results showed that it was advantage of adsorption at solution pH = 4 [32]. Lin et al. [33] explored the phosphorus adsorption onto zeolite/hydrated zirconia, and also indicated that the adsorption performance was best at pH = 2.79. In another study of phosphorus adsorption onto cubic zeolitic imidazolate framework-8, Shams et al. [34] showed that the adsorption was best at solution pH = 2.8. This study is consistent with those studies. In practice, there are many acidic phosphorus-containing wastewaters, such as phosphorus-containing wastewater from phosphorus compound fertilizer processing industry and high-phosphorus wastewater from marine oil and gas pipeline cleaning [35]. Therefore, the pH of the solution was chosen to be 3.0 and used in subsequent studies, taking into account the sorbent utilization and actual wastewater conditions.

3.2.2. Effect of adsorbent dosage

In order to ensure the utilization efficiency of adsorbent and improve its economic benefit, this experiment presents the effect of adsorbent dosage on the phosphate adsorption onto D751-Fe and the results are presented in Fig. 5. It is

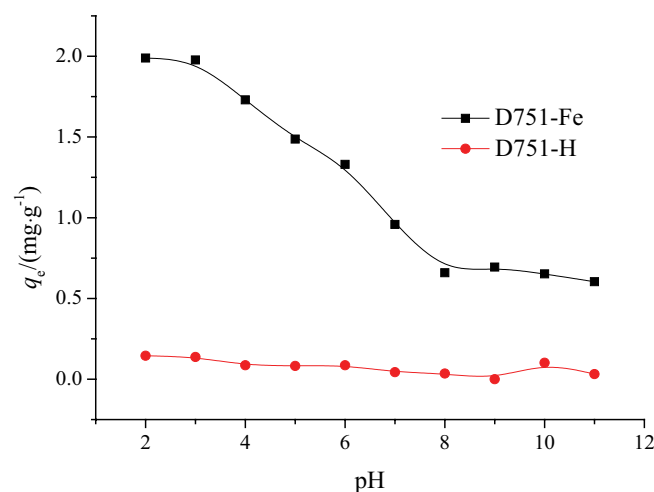


Fig. 4. Effect of pH on phosphate adsorption.

obviously shown from Fig. 5, that the removal efficiency first increased and then stabilized with the increase in the mass of the adsorbent; while the unit adsorption amount gradually decreased. The reason might be that there was more adsorbate that can be combined when adsorbent mass was small, so the unit adsorption amount was large. As the active sites on the adsorbent were limited, resulting in lower removal efficiency. When adsorbent mass increased, the unit adsorption quantity was small, and the active sites on the adsorbent increased correspondingly, and the removal efficiency increased. When the adsorbent mass was 0.1 g, the removal efficiency was as high as 97%, reduced the phosphate content of 10 mg L⁻¹ to less than 0.3 mg L⁻¹. In the following study, mass was chosen to be 0.03 g and the solid–liquid ratio was 1.5 g L⁻¹.

3.2.3. Influence of salinity

The influence of system salinity during adsorption is not negligible. In order to investigate the effect of salinity on the adsorption of phosphate by D751-Fe, NaCl and Na₂SO₄ are selected in this experiment. The results are shown in Fig. 6.

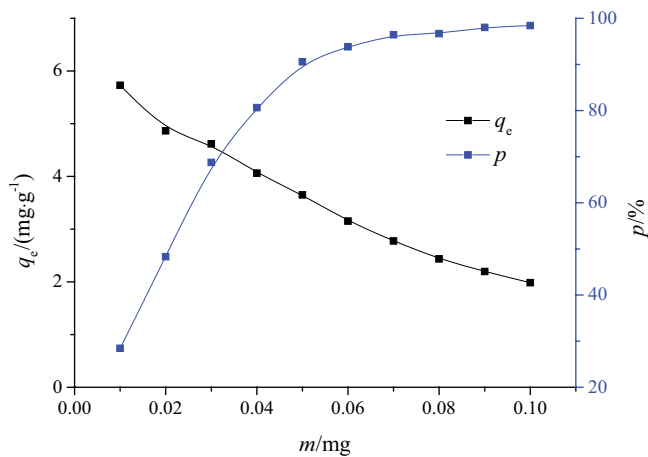


Fig. 5. Effect of the amount of adsorbent on phosphate adsorption.

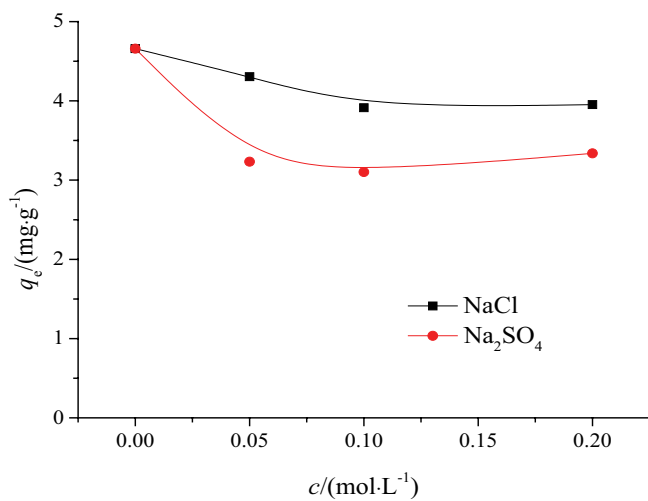


Fig. 6. Effect of salinity on phosphate adsorption.

It is seen from the figure that there was negative effect with existence of SO₄²⁻, which might be the competitive adsorption between SO₄²⁻ and phosphate. However, on the whole, the adsorption quantity of phosphate adsorption onto D751-Fe was not greatly affected by the salinity. This referred that D751-Fe have good salt tolerance. Similar results of phosphorus adsorption were obtained by other studies [1,34].

3.2.4. Adsorption kinetics analysis

In order to further research the adsorption mechanism, this experiment explores the effect of time and initial concentration on the adsorption of phosphate by D751-Fe.

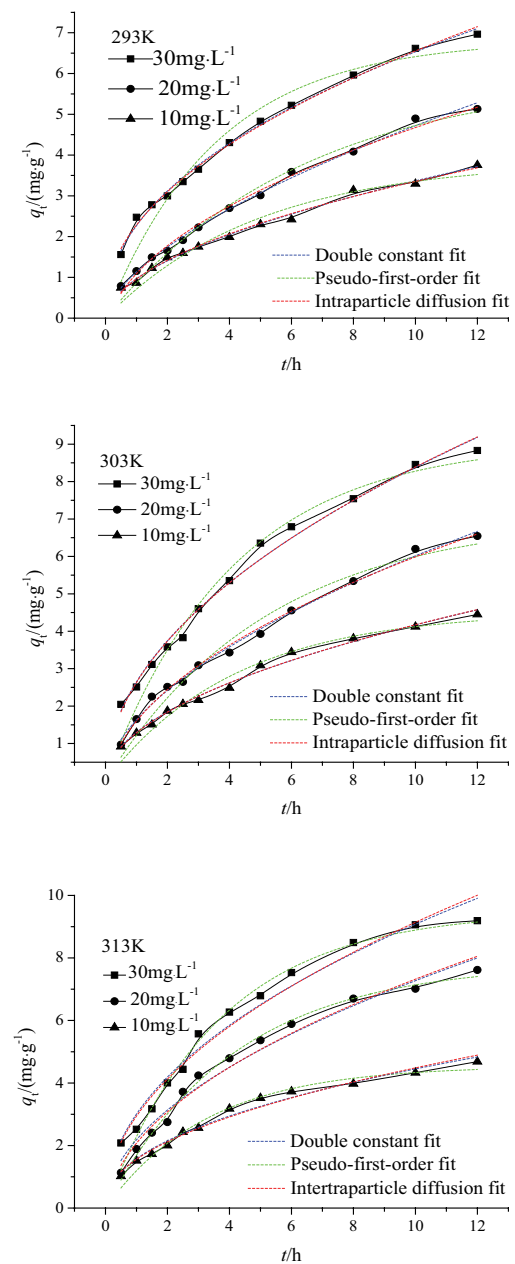


Fig. 7. Adsorption kinetics of phosphate adsorption onto D751-Fe.

The results are illustrated in Fig. 7. It is observed from the figure that values of q_e increased rapidly with the increasing of adsorption time, and finally tended to be slow. This was due to the relatively more active sites that could bind phosphate at the initial stage, so the adsorption was faster; as the active site on the adsorbent decreased, the relatively binding active sites decreased, and the adsorption rate was slower. In addition, the smaller the initial concentration, the shorter the time required for the adsorption to reach equilibrium, because the relatively binding active sites were more for the low concentration of phosphate, which was easy for adsorption to reach equilibrium. On the contrary, there were relatively fewer active sites that could be bound for high concentration of phosphate, the competitive adsorption was fierce and longer time was needed to obtain equilibrium. In this study, four kinetic equations (these models work better than others and corresponding expressions are listed in Table 1) are applied to fit the adsorption curves of three different initial concentrations of phosphate at three different temperatures. Nonlinear regressive analysis is applied. The pseudo-first-order kinetic model is used to describe the adsorption process of physical adsorption rate control. The pseudo-second-order kinetic model is suitable for describing the adsorption process of chemical adsorption rate control. The intraparticle diffusion equation model is often used to determine the rate-determining step and adsorption mechanism of the adsorption process. The double constant equation is an experienced equation applied to describe the heterogeneous diffusion process and reveal the complexity of the adsorption process [36]. The suitability of all kinetic models was judged mainly by comparing R^2 and SSE.

The fitted curves and fitting parameters are presented in Fig. 7 and Table 2, respectively.

It is shown in Table 2 that there were higher values of R^2 (≥ 0.962) and lower values of SSE (≤ 5.54) from the double constant model and the intraparticle diffusion model. This manifested that the adsorption process was a heterogeneous diffusion process combined with chemical adsorption, such

as ion exchange. As there were higher values of R^2 and lower values of SSE from pseudo-first-order kinetic model, the predicted q_e from this model and the experimental q_e were very close. It was also found that both values of k_1 and q_e became larger with the increase in temperature, and this indicated that the adsorption process was an endothermic process. So pseudo-first-order kinetic model could predict the equilibrium adsorption quantity. Although there were higher values of R^2 and lower values of SSE, the pseudo-second-order kinetic model was not suitable for describing the adsorption process because the theoretical value q_e differed greatly from the experimental value q_e .

This implied that there was physical action in the adsorption process. In short, the adsorption process was a complex process in which chemical adsorption and physical adsorption coexisted.

3.2.5. Adsorption isotherm analysis

In the adsorption experiment, the influence of equilibrium concentration and adsorption temperature is usually very important. In order to explore the mechanism, this experiment further performs the effect of equilibrium concentration and temperature on the phosphate adsorption. The results are shown in Fig. 8. It is seen from the figure that when the adsorption temperature was constant, the values of q_e became larger with the increase in phosphate concentration. Finally, adsorption tended to equilibrium. When the equilibrium concentration of the phosphate solution was the same, the higher the adsorption temperature was, the larger values of q_e was, this also revealed that the adsorption process was endothermic.

In this study, three isothermal adsorption models (these models work better than others and corresponding expressions are also listed in Table 1) were used to fit the isotherms of phosphate at three temperatures. The Langmuir model is often used to describe the monolayer adsorption process for uniform surfaces, where K_L is the adsorption equilibrium constant that can be used to reflect the binding force between

Table 1
Several common adsorption models

Models	Nonlinear form	Symbol description
Isotherm model		
Langmuir	$q_e = \frac{q_m K_L C_e}{1 + K_L C_e}$	q_m (mg g ⁻¹) is monolayer theoretical saturated adsorption amount; K_L (L mg ⁻¹) is constant associated with binding energy.
Freundlich	$q_e = K_f C_e^{1/n}$	K_f and $1/n$ are temperature-dependent constants.
Koble–Corrigan	$q_e = \frac{AC^n}{1 + BC^n}$	A and B are equation parameters.
Kinetic model		
Pseudo-first-order kinetic model	$q_t = q_e(1 - e^{-k_1 t})$	k_1 (min ⁻¹) is a quasi-first order rate constant.
Pseudo-second-order kinetic model	$q_t = \frac{k_2 q_e^2 t}{1 + k_2 q_e t}$	k_2 (g mg ⁻¹ min ⁻¹) is a quasi-secondary rate constant.
Intraparticle diffusion	$q_t = k_t t^{1/2} + C$	K_i is the adsorption rate constant; C is the maximum adsorption amount.
Double constant	$\ln q_t = \ln A + K_s t$	A is a constant; K_s is the adsorption rate coefficient.

Table 2
Adsorption kinetics fitting parameters

Pseudo-first-order kinetic model						
T/K	C_0 /(mg L ⁻¹)	$q_{e(\text{exp})}$ /(mg g ⁻¹)	$q_{e(\text{theo})}$ /(mg g ⁻¹)	k_1 /(h ⁻¹)	R ²	SSE
293	10	4.52	4.54 ± 0.15	0.151 ± 0.01	0.974	0.638
	20	7.17	7.89 ± 0.28	0.102 ± 0.008	0.989	0.801
	30	9.38	9.14 ± 0.41	0.157 ± 0.018	0.946	5.05
303	10	5.97	6.06 ± 0.18	0.152 ± 0.011	0.981	0.837
	20	8.80	9.21 ± 0.22	0.135 ± 0.008	0.990	1.05
	30	10.9	11.0 ± 0.3	0.177 ± 0.011	0.982	2.62
313	10	6.69	6.47 ± 0.29	0.153 ± 0.017	0.950	0.988
	20	9.52	9.38 ± 0.20	0.174 ± 0.010	0.988	0.099
	30	12.5	12.7 ± 0.4	0.184 ± 0.012	0.980	0.282
Double constant model						
T/K	C_0 /(mg L ⁻¹)	A	K_s		R ²	SSE
293	10	1.07 ± 0.05	0.475 ± 0.019		0.984	0.388
	20	1.23 ± 0.06	0.578 ± 0.020		0.989	0.738
	30	2.29 ± 0.06	0.457 ± 0.010		0.995	0.440
303	10	1.42 ± 0.07	0.479 ± 0.02		0.983	0.767
	20	1.89 ± 0.13	0.513 ± 0.026		0.976	2.47
	30	2.96 ± 0.19	0.442 ± 0.025		0.968	4.66
313	10	1.56 ± 0.06	0.469 ± 0.015		0.989	0.507
	20	2.43 ± 0.15	0.455 ± 0.024		0.973	2.95
	30	3.18 ± 0.18	0.461 ± 0.022		0.977	4.47
Intraparticle diffusion model						
T/K	C_0 /(mg L ⁻¹)	K_f /(mg g ⁻¹ h ^{-0.5})	C/(mg g ⁻¹)		R ²	SSE
293	10	0.986 ± 0.034	6.98E-2 ± 9.75E-2		0.983	0.421
	20	1.68 ± 0.04	0.581 ± 0.117		0.991	0.604
	30	1.94 ± 0.04	0.392 ± 0.110		0.994	0.539
303	10	1.33 ± 0.05	5.17E-2 ± 0.14		0.981	0.819
	20	2.04 ± 0.08	0.282 ± 0.227		0.978	2.27
	30	2.40 ± 0.12	0.538 ± 0.354		0.962	5.54
313	10	1.39 ± 0.04	0.173 ± 0.112		0.988	0.564
	20	2.09 ± 0.08	0.259 ± 0.282		0.968	3.52
	30	2.78 ± 0.12	0.334 ± 0.340		0.974	5.12
Pseudo-second-order kinetic model						
T/K	C_0 /(mg L ⁻¹)	$q_{e(\text{exp})}$ /(mg g ⁻¹)	$q_{e(\text{theo})}$ /(mg g ⁻¹)	k_2 /(g mg ⁻¹ h ⁻¹)	R ²	SSE
293	10	4.52	5.87 ± 0.22	2.42E-2 ± 3.14E-3	0.984	0.387
	20	7.17	11.1 ± 0.5	7.33E-3 ± 9.50E-4	0.991	0.606
	30	9.38	11.6 ± 0.6	1.33E-2 ± 2.29E-3	0.969	2.89
303	10	5.97	7.88 ± 0.25	1.77E-2 ± 1.90E-3	0.989	0.479
	20	8.80	12.3 ± 0.4	9.54E-3 ± 1.01E-3	0.992	0.876
	30	10.9	14.0 ± 0.4	1.23E-2 ± 3.32E-3	0.987	1.85
313	10	6.69	8.26 ± 0.41	1.79E-2 ± 3.05E-3	0.971	1.37
	20	9.52	11.9 ± 0.2	1.40E-2 ± 8.07E-3	0.997	0.378
	30	12.5	16.2 ± 0.5	9.63E-3 ± 1.01E-3	0.989	2.16

the adsorbent and the adsorbate. The Freundlich model is suitable for describing heterogeneous multi-molecular layer adsorption processes. The Koble–Corrigan model is a combination of the Langmuir model and the Freundlich model and

is a three-parameter model [36]. The suitability of all thermodynamic models is judged mainly by comparing R^2 and SSE. The fitted curves and fitting parameters are shown in Fig. 8 and Table 3, respectively.

It is seen from Table 3 that there was a strong interaction between D751-Fe and phosphate because of $K_L < 1$. Theoretical q_m was closer to experimental q_m , and both increased with the increase in temperature. Furthermore, as there were higher values of R^2 (≥ 0.959) and lower values of SSE (≤ 2.61), the Langmuir model could well describe the adsorption process. It was also found from Table 3 that the K_F value increased with the increase in temperature. The values of $1/n$ were between 0.1 and 0.5 and showed that the adsorption process was easy [11]. Freundlich model could also describe the adsorption process better through comparison values of R^2 (≥ 0.936) and SSE (≤ 7.25). The values of B from Koble–Corrigan model tended to be 0, revealed that the reaction tended to be described by Freundlich model. There were highest values of R^2 (≥ 0.983) and lowest values of SSE (≤ 1.66) from Koble–Corrigan model, furthermore, the fitted curves from this model were closest to experimental curves. So it was implied that Koble–Corrigan model was best to describe

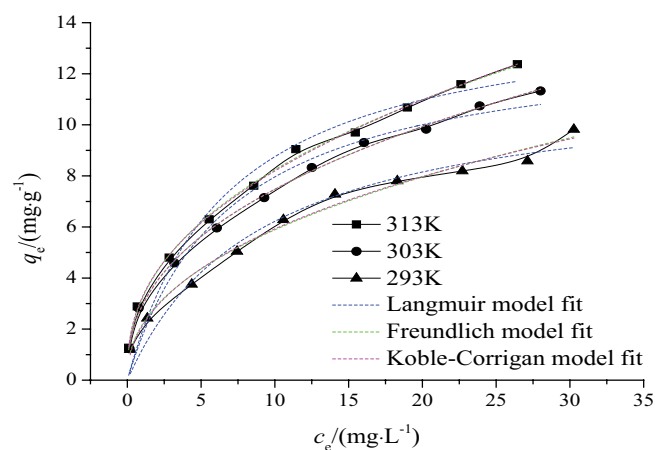


Fig. 8. Adsorption isotherms of phosphate adsorption onto D751-Fe.

Table 3
Adsorption isotherm fitting parameters

Langmuir					
T/K	$K_L/(L\ mg^{-1})$	$q_{e(\text{exp})}/(\text{mg}\ g^{-1})$	$q_{m(\text{theo})}/(\text{mg}\ g^{-1})$	R^2	SSE
293	0.169 ± 0.030	10.9	12.6 ± 0.6	0.959	2.61
303	0.254 ± 0.023	12.6	14.1 ± 0.3	0.988	1.06
313	0.438 ± 0.053	14.07	14.9 ± 0.4	0.978	2.45
Freundlich					
T/K	K_F	$1/n$		R^2	SSE
293	3.29 ± 0.21	0.353 ± 0.022		0.979	1.24
303	4.38 ± 0.35	0.327 ± 0.028		0.959	3.59
313	5.67 ± 0.49	0.290 ± 0.031		0.936	7.25
Koble–Corrigan					
T/K	A	B	n	R^2	SSE
293	3.30 ± 0.27	0.152 ± 0.048	0.549 ± 0.101	0.985	0.782
303	4.29 ± 0.29	0.267 ± 0.019	0.778 ± 0.072	0.994	0.483
313	6.88 ± 0.59	0.417 ± 0.049	0.789 ± 0.111	0.983	1.66

the equilibrium process. This further manifested that the adsorption process was a heterogeneous multi-layer adsorption process, and there was some homogeneous monolayer adsorption process [37]. In other words, the adsorption was a complex process in which single layer uniform adsorption and multiple non-uniform adsorptions coexisted [38–40].

3.2.6. Adsorption thermodynamic parameters

From the change of energy in the adsorption process, the direction of the reaction, the energy required in the reaction process and whether the reaction reaches equilibrium can be revealed. In practice, it can be judged by Gibbs free energy (ΔG), enthalpy change (ΔH), and entropy change (ΔS). The adsorption of phosphate by D751-Fe was an adsorption equilibrium process. The adsorption equilibrium constant (K_c) can be calculated according to Eq. (5).

$$K_c = C_{\text{ad,e}} / C_e \quad (5)$$

Among them, $C_{\text{ad,e}}$ ($\text{mg}\ \text{L}^{-1}$) and C_e ($\text{mg}\ \text{L}^{-1}$) are the concentration of the adsorbate on the adsorbent and the concentration of the adsorbate in the solution when the adsorption is balanced.

Finding K_c and bringing it to Eq. (6) to find the ΔG value.

$$\Delta G = -RT \ln K_c \quad (6)$$

where ΔG represents the Gibbs free energy; R ($8.314\ \text{J}\ \text{mol}^{-1}\ \text{K}^{-1}$) denotes the gas constant; T (K) expresses the absolute temperature; K_c is the adsorption equilibrium constant.

Linear regression is performed on $\Delta G-T$ by Gibbs–Helmholtz equation (Eq. (7)), and ΔH ($\text{kJ}\ \text{mol}^{-1}$) and ΔS ($\text{J}\ \text{mol}^{-1}\ \text{K}^{-1}$) are known from the slope and intercept of the straight line.

Because ΔH , ΔS are a little affected by temperature, it can be regarded as a constant.

$$\Delta G = \Delta H - T\Delta S \quad (7)$$

For the actual system, in addition to considering the possibility of reaction, the reaction rate should also be considered. It can be expressed by activation energy. The apparent activation energy can be obtained by bringing the most consistent kinetic adsorption model parameters into the Arrhenius equation (Eq. (8)).

$$\ln k_1 = -\frac{E_a}{RT} + \ln A \quad (8)$$

where k_1 is the adsorption rate constant, E_a (kJ mol^{-1}) represents the apparent activation energy of the reaction, R ($8.314 \text{ J mol}^{-1} \text{ K}^{-1}$) denotes the gas constant, T (K) expresses the absolute temperature, and A is the temperature influence factor.

According to Eqs. (5)–(8), the relevant thermodynamic parameters for phosphorus adsorption are calculated and shown in Table 4.

It was found from Table 4 that the process was spontaneous with negative values of ΔG° . The adsorption process was endothermic with positive value of ΔH and it was in favor of adsorption at higher temperature. Value of ΔS was positive and this declared that the adsorption process was an irreversible adsorption process with the randomness of the solid–liquid interface increased. The positive value of E_a was between 5 and 40 kJ mol^{-1} , and this indicated that chemisorption was dominant during the adsorption process [41]. In conclusion, it could be speculated that the adsorption reaction was a spontaneous and endothermic reaction with entropy increased [42]. There was both chemical and physical adsorption.

3.2.7. Desorption and regeneration

In the adsorption experiment, the regeneration performance of the adsorbent is often an important indicator for evaluating the performance of the adsorbent [43–45]. Therefore, it is necessary to investigate the regeneration performance of spent D751-Fe. After three times of desorption regeneration with 0.1 mol L^{-1} NaOH, the desorption rates were 96.9%, 93.3%, and 91.5%, respectively, and the regeneration efficiencies were 79.8%, 74.5%, and 70.7%, respectively. The efficiency of desorption and regeneration decreased with the increase of desorption regeneration times, but the decline trend was not obvious. This indicated that D751-Fe had some good reusability. Similar result was obtained about phosphate desorption by zirconium-modified carbon nanotube using NaOH solution [46].

3.2.8. Study on desorption kinetics of D751-Fe

In order to understand the reaction mechanism of the desorption process, analytical kinetic experiments are carried

out, and the results are shown in Fig. 9. It was seen from the figure that the desorption rate increased rapidly with time, and then it reached to equilibrium. This desorption process could be divided into two stages: 0–4 h was a rapid desorption, which was mainly the desorption of static adsorption state P; 4–12 h was a slow reaction process, which was mainly the desorption of concentrated adsorption state P.

The desorption process can be fitted by pseudo-first-order and pseudo-second-order models (the two models work better than others and corresponding expressions are listed in Table 1). The fitted curves and fitting data are shown in Fig. 9 and Table 5, respectively. It is seen from Table 5 that the pseudo-first-order equation model and the pseudo-second-order equation model were both better suitable to predict the kinetic desorption process according to values of R^2 and SSE. Furthermore, the fitted curves from these two models were closer to experimental curve. This implied that there may be ion exchange between phosphate and hydroxide and there be also competitive adsorption. In other words, the desorption process included chemical and physical desorption. Similar results were obtained about 2,4-DCP desorption from spent cationic surfactant modified tree leaves using 75% alcohol [47] and *p*-chlorophenol and *p*-nitrophenol desorption from

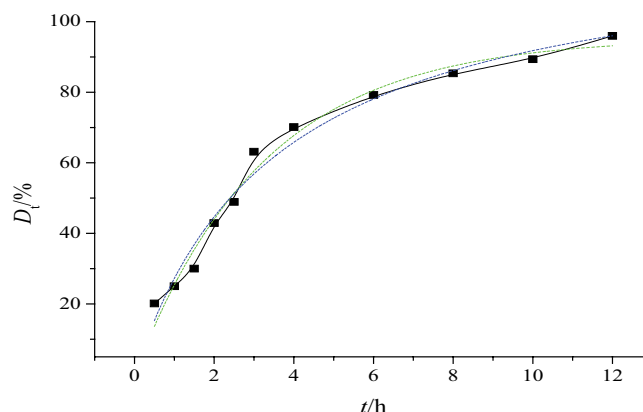


Fig. 9. Desorption kinetics nonlinear fitting curve.

Table 5
Desorption kinetics fitting parameters

Pseudo-first-order kinetic model				
$D_{t(\text{exp})}/\%$	$D_{t(\text{theo})}/\%$	$k_1/(\text{h}^{-1})$	R^2	SSE
96.0	95.5 ± 3.0	0.309 ± 0.024	0.980	131
Pseudo-second-order kinetic model				
$D_{t(\text{exp})}/\%$	$D_{t(\text{theo})}/\%$	$k_2/(\text{g mg}^{-1} \text{h}^{-1})$	R^2	SSE
96.0	125 ± 6	0.00224 ± 3.91	0.977	150

Table 4
Thermodynamic parameters

$E_a/(\text{kJ mol}^{-1})$	$\Delta H/(\text{kJ mol}^{-1})$	$\Delta S/(\text{J mol}^{-1} \text{K}^{-1})$	$\Delta G/(\text{kJ mol}^{-1})$		
			293 K	303 K	313 K
22.4	51.0	179	-1.83	-2.87	-5.42

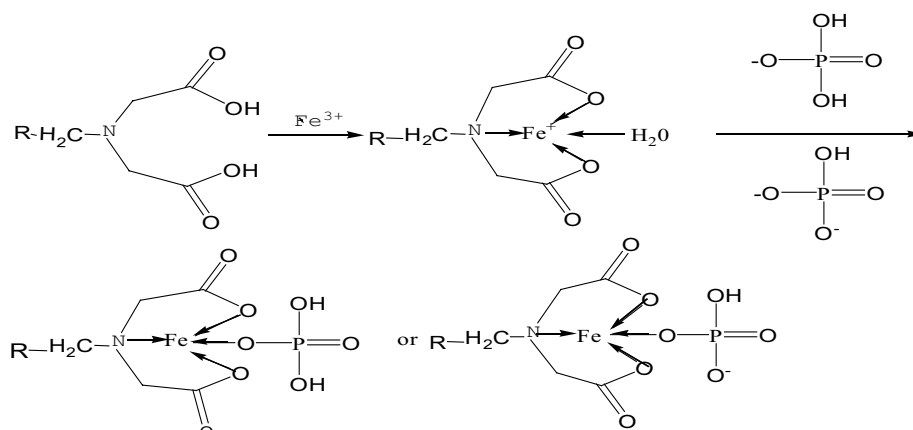


Fig. 10. Adsorption mechanism.

exhausted magnetic activated carbon using 0.01 mol L⁻¹ NaOH solution [48].

3.2.9. Adsorption mechanism

This experiment showed that D751-Fe had a good adsorption effect on phosphate with no adsorption to phosphate by D751-H, indicated that iron loaded on the resin acted on the adsorption toward phosphate. Further, the adsorption effect was good under the solution pH = 3, it was attributed to electrostatic attraction with phosphate mainly present in the form of H₂PO₄⁻ and HPO₄²⁻ with pH in the range of 3–11 [11,30]. In addition, the adsorption process was essentially unaffected by salinity, revealed that Fe on D751-Fe could form a complex with phosphate. In summary, it was speculated that the adsorption mechanism was mainly a combination of physical adsorption (electrostatic attraction) and chemical adsorption (coordination reaction) between D751-Fe and phosphate [44]. The mechanism of action between D751-Fe and phosphate is shown in Fig. 10.

4. Conclusions

The adsorption performance of D751 modified by FeCl₃ was obviously improved. Solid–liquid ratio was 1.5 g L⁻¹, the adsorption time was 18 h, and it was favorable for adsorption under acidic conditions. Salinity had a little effect on adsorption. The isotherm fitting results showed that the adsorption was a complex process containing single layer uniform adsorption and multiple non-uniform adsorptions. The results of kinetic fitting manifested that the adsorption process included chemical adsorption and physical adsorption. Thermodynamic parameters indicated that the adsorption reaction was a spontaneous and endothermic reaction with entropy increased. In addition, D751-Fe had good regeneration performance. It is promising as adsorbent to remove phosphate from solution.

References

- [1] Y. Gu, D.H. Xie, Y. Ma, W.X. Qin, H.M. Zhang, G.Z. Wang, Y.X. Zhang, H.J. Zhao, Size modulation of zirconium-based metal organic frameworks for highly efficient phosphate remediation, *ACS Appl. Mater. Interfaces*, 9 (2017) 32151–32160.
- [2] A. Othman, E. Dumitrescu, D. Andreescu, S. Andreescu, Nanoporous sorbents for the removal and recovery of phosphorus from eutrophic waters: sustainability challenges and solutions, *ACS Sustain. Chem. Eng.*, 6 (2018) 12542–12561.
- [3] Y. Zhang, X.M. Guo, Y. Yao, F. Wu, C.Z. Zhang, R.J. Chen, J. Lu, K. Amine, Mg-enriched engineered carbon from lithium-ion battery anode for phosphate removal, *ACS Appl. Mater. Interfaces*, 8 (2016) 2905–2909.
- [4] M. Kim, H. Kim, S.H. Byeon, Layered yttrium hydroxide 1-Y(OH)₃ luminescent adsorbent for detection and recovery of phosphate from water over a wide pH range, *ACS Appl. Mater. Interfaces*, 9 (2017) 40461–40470.
- [5] C.M. Nobile, M.N. Bravin, E. Tillard, T. Becquer, J.M. Paillat, Phosphorus sorption capacity and availability along a toposequence of agricultural soils: effects of soil type and a decade of fertilizer applications, *Soil Use Manage.*, 34 (2018) 461–471.
- [6] E. Martin, J. Lalley, W.H. Wang, M.N. Nadagouda, E. Sahle-Demessie, S.R. Chae, Phosphate recovery from water using cellulose enhanced magnesium carbonate pellets: kinetics, isotherms, and desorption, *Chem. Eng. J.*, 352 (2018) 612–624.
- [7] Y.C. Liu, H.C. Shi, W.L. Li, Y.L. Hou, M. He, Inhibition of chemical dose in biological phosphorus and nitrogen removal in simultaneous chemical precipitation for phosphorus removal, *Bioresour. Technol.*, 102 (2011) 4008–4012.
- [8] H.M. Zou, Y. Wang, Phosphorus removal and recovery from domestic wastewater in a novel process of enhanced biological phosphorus removal coupled with crystallization, *Bioresour. Technol.*, 211 (2016) 87–92.
- [9] M. Reza, M.A. Cuenca, Simultaneous biological removal of nitrogen and phosphorus in a vertical bioreactor, *J. Environ. Chem. Eng.*, 4 (2016) 130–136.
- [10] M.L. Chen, C.B. Huo, Y.K. Li, J.H. Wang, Selective adsorption and efficient removal of phosphate from aqueous medium with graphene–lanthanum composite, *ACS Sustain. Chem. Eng.*, 4 (2016) 1296–1302.
- [11] R. Xue, J. Xu, L. Gu, L.H. Pan, Q. He, Study of phosphorus removal by using sponge iron adsorption, *Water Air Soil Pollut.*, 229 (2018) 1–12.
- [12] S.Y. Yoon, C.G. Lee, J.A. Park, J.H. Kim, S.B. Kim, S.H. Lee, J.W. Choi, Kinetic, equilibrium and thermodynamic studies for phosphate adsorption to magnetic iron oxide nanoparticles, *Chem. Eng. J.*, 236 (2014) 341–347.
- [13] X.H. Liu, E. Zong, W.J. Hu, P.G. Song, J.F. Wang, Q.C. Liu, Z.Q. Ma, S.Y. Fu, Lignin-derived porous carbon loaded with La(OH)₃ nanorods for highly efficient removal of phosphate, *ACS Sustain. Chem. Eng.*, 7 (2019) 758–768.
- [14] J. Qu, Y.L. Liu, Y. Wang, Study on the adsorption properties of cesium hydroxide on phosphate, *Shandong Chem. Industry (in Chinese)*, 47 (2018) 10–12.

- [15] J.W. Kim, I.J. Hwang, Separation of valuables from spent selective catalytic reduction catalyst leaching solution by fabricated anion extraction resins, *J. Environ. Chem. Eng.*, 6 (2018) 1100–1108.
- [16] Y. Wu, Y.B. Han, Y. Tao, S.Q. Fan, D.T. Chu, X.S. Ye, M.R. Ye, G.J. Xie, Ultrasound assisted adsorption and desorption of blueberry anthocyanins using macroporous resins, *Ultrason. Sonochem.*, 48 (2018) 311–320.
- [17] J.L. Wang, X.H. Wen, D. Zhou, Production of citric acid from molasses integrated with in-situ product separation by ion-exchange resin adsorption, *Bioresour. Technol.*, 75 (2000) 231–234.
- [18] W.J. Sun, D.B. Yue, J.G. Song, Y.F. Nie, Adsorption removal of refractory organic matter in bio-treated municipal solid waste landfill leachate by anion exchange resins, *Waste Manage.*, 81 (2018) 61–70.
- [19] X.B. Zhu, W. Li, Q. Zhang, C.X. Zhang, L.J. Chen, Separation characteristics of vanadium from leach liquor of red mud by ion exchange with different resins, *Hydrometallurgy*, 176 (2018) 42–48.
- [20] G.J. Millar, S.J. Couperthwaite, D.B. Wellner, D.C. Macfarlane, S.A. Dalzell, Removal of fluoride ions from solution by chelating resin with imino-diacetate functionality, *J. Water Process Eng.*, 20 (2017) 113–122.
- [21] Y.X. Liu, X. Hua, M.M. Wang, R.J. Yang, Purification of the mother liquor sugar from industrial stevia production through one-step adsorption by non-polar macroporous resin, *Food Chem.*, 274 (2019) 337–344.
- [22] B.M. Xie, J.N. Zuo, L.L. Gan, F.L. Liu, K.J. Wang, Cation exchange resin supported nanoscale zero-valent iron for removal of phosphorus in rainwater runoff, *Front. Environ. Sci. Eng.*, 8 (2014) 463–470.
- [23] Z.P. Ye, H.W. Li, Y. Lin, Removal and recovery of phosphorus from eutrophic river water by resin method, *Environ. Eng. J. (in Chinese)*, 7 (2013) 3025–3030.
- [24] J.J. Song, P.P. Huang, L.F. Chen, Z.W. Qi, J.G. Yu, Adsorption properties and mechanism of D751 resin for lithium ion, *Chem. Ind. E. Progress (in Chinese)*, 31 (2012) 370–375.
- [25] A. Ramirez, S. Giraldo, J. Garcia-Nunez, E. Flórez, N. Acelas, Phosphate removal from water using a hybrid material in a fixed-bed column, *J. Water Process Eng.*, 26 (2018) 131–137.
- [26] H.S. Liang, S.J. Chen, G.S. Liu, X.D. Hou, Study on removal of lead, cadmium and copper from radix isatidis decoction by D751 resin column, *Anhui Agric. Sci. (in Chinese)*, 40 (2012) 2144–2146.
- [27] M. Arshadi, M.K. Abdolmaleki, H. Eskandarloo, M. Azizi, A. Abbaspourrad, Synthesis of highly monodispersed, stable, and spherical NZVI of 20–30 nm on filter paper for the removal of phosphate from wastewater: batch and column study, *ACS Sustain. Chem. Eng.*, 6 (2018) 11662–11676.
- [28] Z.S. Liu, Y. Zhang, B.Y. Liu, L. Zeng, D. Xu, F. He, L.W. Kong, Q.H. Zhou, Z.B. Wu, Adsorption performance of modified bentonite granular (MBG) on sediment phosphorus in all fractions in the west lake, *J. Ecol. Eng.*, 106 (2017) 124–131.
- [29] M. Zhang, L. Wang, H.Y. Li, N. Hu, D. Liu, G.D. Tang, L.X. Wang, Preparation and denitrification performance of novel modified resin adsorbents, *Appl. Chem. Ind. (in Chinese)*, 45 (2016) 680–683.
- [30] X.Q. Li, J. Cui, Y.S. Pei, Granulation of drinking water treatment residuals as applicable media for phosphorus removal, *J. Environ. Manage.*, 213 (2018) 36–46.
- [31] M. Mallet, K. Barthelemy, C. Ruby, A. Renard, S. Naille, Investigation of phosphate adsorption onto ferrihydrite by X-ray photoelectron spectroscopy, *J. Colloid Interface Sci.*, 407 (2013) 95–101.
- [32] X.N. Zhang, X.Y. Lin, Y. He, Y. Chen, J. Zhou, X.G. Luo, Adsorption of phosphorus from slaughterhouse wastewater by carboxymethyl konjac glucomannan loaded with lanthanum, *Int. J. Biol. Macromol.*, 119 (2018) 105–115.
- [33] L.D. Lin, Z. Wang, W. Gu, D.Y. Wu, The adsorption of phosphorus from water by zeolite/hydrated zirconia, *Environ. Eng. J. (in Chinese)*, 11 (2017) 702–708.
- [34] M. Shams, M.H. Dehghani, R. Nabizadeh, A. Mesdaghinia, M. Alimohammadi, A.A. Najafpoor, Adsorption of phosphorus from aqueous solution by cubic zeolitic imidazolate framework-8: Modeling, mechanical agitation versus sonication, *J. Mol. Liq.*, 224 (2016) 151–157.
- [35] Z.Y. Jia, Z.G. Wang, P.G. Cheng, Z.L. Xiang, N. Tang, Study on the process optimization of high phosphorus cleaning wastewater in marine oil and gas pipeline by Fenton method, *Water Treat. Tech. (in Chinese)*, 40 (2014) 83–86.
- [36] M.Y. Han, Q. Wang, H. Li, L.Y. Fang, R.P. Han, Removal of methyl orange from aqueous solutions by polydopamine-mediated surface functionalization of Fe₃O₄ in batch mode, *Desal. Wat. Treat.*, 115 (2018) 271–280.
- [37] Y.Y. Hu, R.P. Han, Selective and efficient removal of anionic dyes from solution by zirconium(IV) hydroxide-coated magnetic materials, *J. Chem. Eng.*, 64 (2019) 791–799.
- [38] X.Y. Yang, X.W. Chen, X.T. Yang, Effect of organic matter on phosphorus adsorption and desorption in a black soil from Northeast China, *Soil Till. Res.*, 187 (2019) 85–91.
- [39] M. Kasprzyk, M. Gajewska, Phosphorus removal by application of natural and semi-natural materials for possible recovery according to assumptions of circular economy and closed circuit of P, *Sci. Total Environ.*, 650 (2019) 249–256.
- [40] Y. Zhang, X.M. Guo, F. Wu, Y. Yao, Y.F. Yuan, X.X. Bi, X.Y. Luo, R. Shahbazian-Yassar, C.Z. Zhang, K. Amine, Mesocarbon microbead carbon-supported magnesium hydroxide nanoparticles: turning spent Li-ion battery anode into a highly efficient phosphate adsorbent for wastewater treatment, *ACS Appl. Mater. Interfaces*, 8 (2016) 21315–21325.
- [41] R.P. Han, J.J. Zhang, P. Han, Y.F. Wang, Z.H. Zhao, M.S. Tang, Study of equilibrium, kinetic and thermodynamic parameters about methylene blue adsorption onto natural zeolite, *Chem. Eng. J.*, 145 (2009) 496–504.
- [42] F.Z. Xie, Z.L. Dai, Y.R. Zhu, G.L. Li, H.B. Li, Z.Q. He, S.X. Geng, F.C. Wu, Adsorption of phosphate by sediments in a eutrophic lake: isotherms, kinetics, thermodynamics and the influence of dissolved organic matter, *Colloids Surf., A*, 562 (2019) 16–25.
- [43] R.D. Zhang, J.H. Zhang, X.N. Zhang, C.C. Dou, R.P. Han, Adsorption of Congo red from aqueous solutions using cationic surfactant modified wheat straw in batch mode: kinetic and equilibrium study, *J. Taiwan Inst. Chem. Eng.*, 45 (2014) 2578–2583.
- [44] Y.F. Gu, M.Y. Liu, M.M. Yang, W.L. Wang, S.S. Zhang, R.P. Han, Adsorption of light green anionic dye from solution using polyethyleneimine-modified carbon nanotubes in batch mode, *Desal. Wat. Treat.*, 138 (2019) 368–378.
- [45] B.L. Zhao, W. Xiao, Y. Shang, H.M. Zhu, R.P. Han, Adsorption of light green anionic dye using cationic surfactant-modified peanut husk in batch mode, *Arab. J. Chem.*, 10 (2017) s3595–s3602.
- [46] Y.F. Gu, M.M. Yang, W.L. Wang, R.P. Han, Phosphate adsorption from solution by zirconium loaded carbon nanotubes in batch mode, *J. Chem. Eng. Data*, 64 (2019) 2849–2858.
- [47] X.F. Ren, R.D. Zhang, W.Z. Lu, T. Zhou, R.P. Han, S.S. Zhang, Adsorption potential of 2,4-dichlorophenol onto cationic surfactant-modified Phoenix tree leaf in batch mode, *Desal. Wat. Treat.*, 57 (2016) 6333–6346.
- [48] Y.C. Rong, R.P. Han, Adsorption of p-chlorophenol and p-nitrophenol in single and binary systems from solution using magnetic activated carbon, *Korean J. Chem. Eng.*, 36 (2019) 942–953.